The Impact of Silicon Solar Cell Architecture and Cell Interconnection on Energy Yield in Hot & Sunny Climates

Jan Haschke,[*a] Johannes P. Seif,[a] Yannick Riesen,[a] Andrea Tomasi,[a] Jean Cattin,[a] Loïc Tous,[b] Patrick Choulat,[b] Monica Aleman,[b] Emanuele Cornagliotti,[b] Angel Uruena,[b] Richard Russell,[b] Filip Duerinckx,[b] Jonathan Champliaud,[c] Jacques Levrat,[c] Amir A. Abdallah,[d] Brahim Aïssa,[d] Nouar Tabet,[d] Nicolas Wyrsch,[a] Matthieu Despeisse,[c] Jozef Szlufcik,[b] Stefaan De Wolf,[a,‡] Christophe Ballif,[a,c]

[*] *Corresponding author. Tel: +41 21 69 54384; Fax: +41 21 695 42 01; E-mail: jan.haschke@epfl.ch*

[a] *Ecole Polytechnique Fédérale de Lausanne, Institute of Microengineering (IMT), Photovoltaics and Thin-Film Electronics Laboratory (PV-lab), Rue de la Maladière 71B, CH-2002 Neuchâtel, Switzerland.*

[b] *Interuniversity Microelectronics Center (imec), Kapeldreef 75, BE-3001 Leuven, Belgium.*

[c] *Swiss Center for Electronics and Microtechnology (CSEM), PV-center, Rue Jaquet Droz 1, CH-2002 Neuchâtel, Switzerland.*

[d] *Qatar Environment and Energy Research Institute (QEERI), Hamad bin Khalifa University, Qatar Foundation, P.O. Box 5825, Doha, Qatar.*

[‡] *Present address: King Abdullah University of Science and Technology (KAUST), KAUST Solar Center (KSC), Thuwal, 23955-6900, Saudi Arabia*

1 Calculation of annual energy production

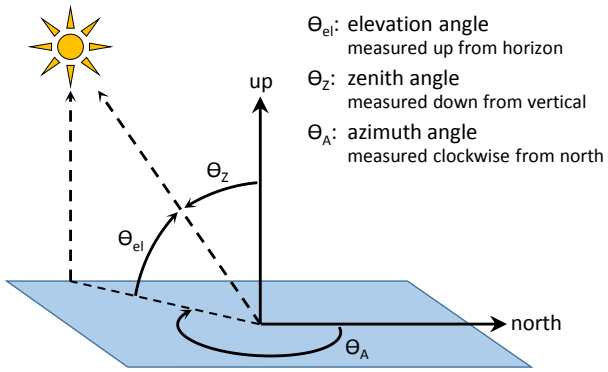

Figure 1: Schematic of elevation, zenith, and azimuth angles. Sketched after: https://pvpmc.sandia.gov/modeling-steps/1-weather-design-inputs/sun-position/.

To calculate annual energy production, we used weather data provided by the American Society of Heating, Refrigerating and Air-Conditioning Engineers (ASHRAE)[1]. The data describe a typical meteorological year and include the global horizontal irradiance (GHI), diffuse horizontal irradiance (DHI), as well as air temperature and wind speed at the given location in hourly timesteps.

The module plane is tilted south (azimuth angle $\Theta_A = 180°$) by 40° (Geneva) and 30° (Abu Dhabi). These angles were chosen as they led to the highest annual energy production when the tilt angle was varied in 5°-steps. The effective in-plane irradiance and the module temperature were calculated using the weather data and several functions provided by the PV-lib toolbox[1]. The direct compound of the effective in-plane irradiance was calculated using trigonometry and the direct normal irradiance (DNI) according to

$$\mathrm{DNI} = \frac{\mathrm{GHI} - \mathrm{DHI}}{\cos(\Theta_Z)} \tag{1}$$

with GHI and DHI taken from the weather data and the zenith angle, Θ_Z. Θ_Z was calculated using the function *pvl_ephemeris*, which calculates the elevation and azimuth angle of the sun for a given location and time (see Fig. 1). Losses of the direct irradiation component due to an angle of incidence differing from the surface normal where taken into account based on the Sandia PV Array Performance model[3] using the polynom coefficients of the SunPower SP-305-WHT module. The diffuse component of the effective in-plane irradiance is a sum of the diffuse irradiance according to the King model[4], calculated with the function *pvl_kingdiffuse* and the diffuse irradiance from ground reflection. The latter was calculated using the Lutzenhiser model[5], an albedo of 0.2 and the function *pvl_grounddiffuse*. For both direct and diffuse irradiation, irradiance losses due to an enhanced air mass where taken into account based on the Sandia PV Array Performance model[3] using the polynom coefficients of the SunPower SP-305-WHT module. The air mass was calculated with the function *pvl_relativeairmass* using the model of Gueyard[6].

The temperature of the solar cell was calculated as a function of the ambient temperature, effective in-plane irradiance and windspeed using the function *pvl_sapmcelltemp*.

Together with the irradiance- and temperature-dependent power output for each solar cell, determined from temperature- and irradiance-dependent $J(V)$ measurements, the produced energy per time step was calculated.

2 Detailed description of J(V,T) measurement

To ensure accurate determination of temperature coefficients (TCs) from temperature-dependent $J(V)$ measurements, (i) the difference between two temperatures must be accurately known and (ii) the temperature of the solar cell during the measurement must be constant when measuring J_{SC}, P_{MPP}, and V_{OC}.

To determine the **accurate difference between two temperature steps**, the temperature of the chuck's surface was measured at five positions at the center and the corners of a 135 mm x 135 mm square with a resistance thermometer (Pt100) and compared with the value measured with another Pt100 inside the chuck. We found that, in our system, the chuck surface's temperature at a set value of 25 °C was on average 25.7 °C, while at 65 °C it was 64.7 °C. The standard deviation increased with increasing temperature (see Table 1). For the analysis of all measurements using this chuck, the temperature was corrected accordingly. When needed, the values for 25 °C or 75 °C were obtained using linear extrapolation.

[1]The PV-lib toolbox[2] is a set of functions thet calculate the performance of photovoltaic energy systems. It is available as Matlab or Python code. It was developed at Sandia National Laboratories.

To ensure that the **temperature of the solar cell during the measurement** remained constant, the solar cell was placed on a temperature-controlled chuck. Without illumination, the temperature of the solar cell is equal to the temperature of the surface of the chuck. Under illumination, dependent upon the thermal coupling between the chuck and the cell, the temperature of the cell can be higher than the temperature of the chuck. Under both V_{OC} and J_{SC} conditions, no power is transferred to the external circuit and heating is most pronounced. As shown by simulations by Couderc *et al.*[7], the stabilized temperature of the solar cell is the same for either of these two conditions. Under maximum power point (MPP) conditions, however, part of the energy is transferred to the external circuit. Less power is therefore available to heat the cell and the stabilized temperature of the cell is lower[7].

To examine the heating of the cell under illumination and V_{OC} conditions, we first determined the TC of the V_{OC} ($TC_{V_{OC}}$) as follows. At each temperature, the V_{OC} was measured as a function of time. When the shutter of the solar simulator opened, the V_{OC} rose to a maximum until the shutter was fully open. This was followed by a decrease in the V_{OC} as the temperature of the solar cell increased. The maximum value of the $V_{OC}(t)$ curve (V_{OC}^{max}) is then considered to be the correct V_{OC} at the given temperature and used to calculate the temperature coefficient, $TC_{V_{OC}}$. The values for the $TC_{V_{OC}}$ obtained by this method and the ones obtained from $J(V)$ measurements are listed in Table 2. The data show that the same $TC_{V_{OC}}$ is obtained by both methods. Minor differences were arbitrarily observed in some architectures and considered to be caused by the uncertainty of the measurements.

When the temperature coefficient of the V_{OC} of a solar cell is known, the temperature of the cell can be calculated from the measured V_{OC}. Using this $TC_{V_{OC}}$ and the $V_{OC}(t)$ characteristics, the temperature versus time of the investigated solar cells under STC irradiance (AM1.5g, $1000\,W\,m^{-2}$) was calculated as shown in Fig. 2a. It can be seen that the *p*-PERC and the *n*-SHJ cell heat up approximately 0.5 °C more during the first second of STC irradiation. Thereafter, the increase in cell temperature over time is similar to the other cells. The reason for the faster temperature increase during the first second is the thermal coupling of the cell to the chuck. The rear sides of both the *p*-PERC and the *n*-SHJ solar cells rear sides are not as smooth as the rear sides of the other cells, which can be seen in the profilometer line scans shown in Fig. 2b. In the *p*-PERC cell, this is due to roughness caused by the laser-fired contacts at the rear; for the bifacial *n*-SHJ cell, the rear grid prevents good thermal coupling. The reason for the constant, albeit slow, increase in cell temperature during illumination of 50 s is most likely from how the chuck temperature is controlled by the temperature controller.

The $J(V)$ measurements were taken by biasing the solar cells from reverse (-1 V) to forward

Table 1: Surface temperatures in °C of the chuck used for the $J(V)$ measurements, measured with a Pt100 at five different positions (T: top, B: bottom, R: right, L: left, C: center). The temperature used for the correction of the temperature is ϑ_{avg}^{surf}

ϑ_{set}	ϑ_{TL}^{surf}	ϑ_{TR}^{surf}	ϑ_{C}^{surf}	ϑ_{BL}^{surf}	ϑ_{BR}^{surf}	ϑ_{avg}^{surf}
25.0	25.6	25.7	25.7	25.6	25.7	**25.7 ± 0.1**
35.0	35.4	35.5	35.5	35.2	35.3	**35.4 ± 0.1**
45.0	45.1	45.2	45.3	44.8	44.9	**45.1 ± 0.2**
55.0	54.9	55.0	55.2	54.5	54.9	**54.7 ± 0.3**
65.0	64.8	65.0	65.2	64.2	64.2	**64.7 ± 0.5**

Table 2: Overview of the temperature coefficient of the open-circuit voltage ($TC_{V_{OC}}$) derived from two measurements ($J(V)$ and $V_{OC}(t)$). From $V_{OC}(t)$, $TC_{V_{OC}}$ was calculated using the maxima of the V_{OC} at each temperature.

architecture	$V_{OC}^{J(V)}$ (mV)	V_{OC}^{max} (mV)	$TC_{V_{OC}}^{J(V)}$ (%/K)	$TC_{V_{OC}}^{max}$ (%/K)
p-BSF	640	635	-0.31	-0.31
p-PERC	655	653	-0.29	-0.29
std. *n*-PERT	677	675	-0.28	-0.27
adv. *n*-PERT	687	686	-0.27	-0.27
n-hybrid	678	677	-0.29	-0.28
n-SHJ	733	733	-0.25	-0.24

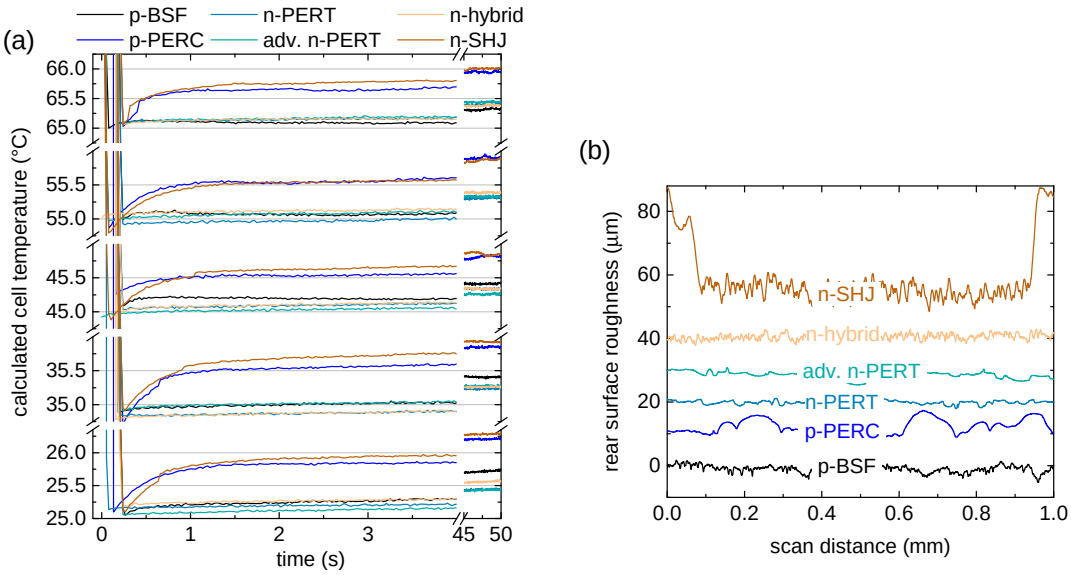

Figure 2: (a) Temperature of the investigated cells under STC irradiance (AM1.5g, 1000 W m^{-2}), calculated from the measured V_{OC} versus time and $TC_{V_{OC}}$. (b) Profilometer line scans on the rear surface of the investigated solar cells. The thermal coupling to the chuck of the *n*-SHJ and the *p*-PERC cell is worse compared with the other cells due to a rear side grid (*n*-SHJ, bifacial) and increased surface roughness caused by laser-fired contacts (*p*-PERC).

(1 V). The voltage sweep started after a waiting time of 300 ms to ensure that the shutter of the solar simulator was fully open. The sum of this waiting time and the sweep time from −1 V to 0 V is approximately 1 s, which allows for sufficient stabilisation of the temperature of the solar cells until the working conditions of interest (J_{SC}, MPP, and V_{OC}) are reached (cf. Fig. 2a). We assume that the cells' temperature are constant during the measurement because the time during which heating is a little less pronounced (under MPP conditions) is very short.

Finally, as the $TC_{V_{OC}}$ obtained from the $J(V)$ measurements and the one obtained from $V_{OC}(t)$ measurements are the same within the margin of measurement accuracy, we consider the values obtained from the $J(V)$ measurements as correct and use them for our further analysis.

3 Derivation of Equation (8)

In this section, we derive equation (8) of the manuscript. Analogous to equation (1) in the manuscript, the relative temperature coefficient of the power at maximum power point ($TC_{P_{MPP}}$) depends on the relative temperature coefficients of both current and voltage at MPP ($TC_{P_{MPP}} = TC_{V_{MPP}} + TC_{J_{MPP}}$). The relative temperature coefficient of V_{MPP} can be written as

$$TC_{V_{MPP}} = \frac{1}{V_{MPP}^{25\,^\circ C}} \cdot \frac{\Delta V_{MPP}}{\Delta T} \ . \tag{2}$$

When going from cell to module, the additional series resistance, R_{CTM}, induced by the cell interconnections reduces the voltage at MPP with respect to V_{MPP} of the cell. When R_{CTM} is small ($< 2\,\Omega\,cm^2$), the reduction of J_{MPP} due to R_{CTM} is negligible. The voltage at MPP of a cell in a module can thus be written as

$$V_{MPP}^{module} = V_{MPP}^{cell} - R_{CTM} \cdot J_{MPP}^{cell} \ . \tag{3}$$

Taking the total derivative of (3) with respect to the temperature, T, leads to

$$\Delta V_{MPP}^{module} = \Delta V_{MPP}^{cell} - R_{CTM} \cdot \Delta J_{MPP}^{cell} - \Delta R_{CTM} \cdot J_{MPP}^{cell} - \Delta R_{CTM} \cdot \Delta J_{MPP}^{cell} \ , \tag{4}$$

where $\Delta J_{MPP}^{cell} = 0$, i.e., $TC_{J_{MPP}} = 0$, which is generally the case for the solar cells investigated in this study. This reduces equation (4) to

$$\Delta V_{MPP}^{module} = \Delta V_{MPP}^{cell} - \Delta R_{CTM} \cdot J_{MPP}^{cell} \ . \tag{5}$$

Using equations (2), (3) and (5), we can write the $TC_{V_{MPP}}$ of a module as

$$TC_{V_{MPP}}^{module} = \frac{1}{V_{MPP}^{cell,25\,^\circ C} - R_{CTM}^{25\,^\circ C} \cdot J_{MPP}^{cell,25\,^\circ C}} \cdot \frac{\Delta V_{MPP}^{cell} - \Delta R_{CTM} \cdot J_{MPP}^{cell}}{\Delta T} \ , \tag{6}$$

which completely depends on cell quantities and R_{CTM}. Furthermore, we define the following equations:

$$\Delta R_{CTM} = R_{CTM}^{25\,^\circ C} \cdot TC_{R_{CTM}} \cdot \Delta T, \tag{7}$$

$$\Delta V_{MPP}^{cell} = V_{MPP}^{cell,25\,^\circ C} \cdot TC_{V_{MPP}}^{cell} \cdot \Delta T, \tag{8}$$

$$J_{\mathrm{MPP}} = \frac{V_{\mathrm{MPP}}}{R_{\mathrm{MPP}}} \,. \tag{9}$$

With the equations (7), (8), and (9), equation (6) can be written as

$$\mathrm{TC}^{\mathrm{module}}_{V_{\mathrm{MPP}}} = \mathrm{TC}^{\mathrm{cell}}_{V_{\mathrm{MPP}}} \frac{R^{25\,^\circ\mathrm{C}}_{\mathrm{MPP}}}{R^{25\,^\circ\mathrm{C}}_{\mathrm{MPP}} - R^{25\,^\circ\mathrm{C}}_{\mathrm{CTM}}} - \mathrm{TC}_{R_{\mathrm{CTM}}} \frac{R^{25\,^\circ\mathrm{C}}_{\mathrm{CTM}}}{R^{25\,^\circ\mathrm{C}}_{\mathrm{MPP}} - R^{25\,^\circ\mathrm{C}}_{\mathrm{CTM}}} \tag{10}$$

As we defined $\mathrm{TC}^{\mathrm{cell}}_{J_{\mathrm{MPP}}} = 0$ (see above) and thus $\mathrm{TC}^{\mathrm{cell}}_{V_{\mathrm{MPP}}} = \mathrm{TC}^{\mathrm{cell}}_{P_{\mathrm{MPP}}}$, equation (10) is equivalent to equation (8) in the manuscript.

4 Additional results from energy yield calculations

In Table 3, the yield (Y_{A}) as defined in equation (9) in the manuscript and the performance ratios (PR) of all investigated solar cell architectures are given for the two locations and with additional R_{CTM} of 1.5 Ω cm^2. The performance ratio was calculated as defined in IEC 61724[8] ($\mathrm{PR} = Y_{\mathrm{A}}/Y_{\mathrm{ref}}$, where Y_{ref} is the reference yield, which is defined as the in-plane irradiance multiplied by the efficiency of the module at STC). It can be seen that both Y_{A} as well as PR increase when there is additional series resistance, while the actually produced energy decreases with increasing $R^{25\,^\circ\mathrm{C}}_{\mathrm{CTM}}$ (cf. Fig. 3). The reason for this is discussed in section 3.5 in the manuscript. Thus, neither Y_{A} nor PR are suitable measures to capture the influence of R_{CTM}. Instead, we chose $\mathrm{EPRP}_{\mathrm{cell}}$ as defined in equation (10) in the manuscript. Nevertheless, we included the yield and PR data here in the supplementary information as they might be of interest to some readers.

Table 3: Comparison of the yield (Y_{A}) of the different architectures, as well as the performance ratio PR, calculated with and without an additional temperature-dependent $R^{25\,^\circ\mathrm{C}}_{\mathrm{CTM}}$ of 1.5 Ω cm^2 for the two studied climates.

architecture	Y_{A} (kWh/kW)		PR	
$R^{25\,^\circ\mathrm{C}}_{\mathrm{CTM}} \rightarrow$	none	1.5 Ω cm^2	none	1.5 Ω cm^2
	Geneva			
p-BSF	1286	1328	0.95	0.98
p-PERC	1285	1328	0.95	0.98
n-PERT	1285	1327	0.95	0.98
adv. *n*-PERT	1281	1323	0.95	0.98
n-hybrid	1279	1321	0.94	0.97
n-SHJ	1300	1338	0.96	0.99
	Abu Dhabi			
p-BSF	1994	2005	0.90	0.90
p-PERC	2003	2016	0.90	0.91
n-PERT	2014	2028	0.91	0.91
adv. *n*-PERT	2008	2023	0.90	0.91
n-hybrid	1994	2009	0.90	0.90
n-SHJ	2062	2079	0.93	0.94

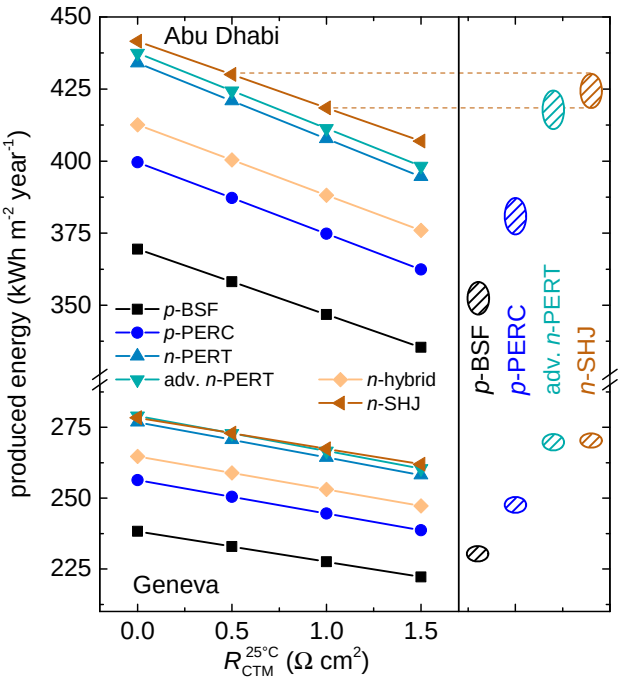

Figure 3: Yearly energy production for temperate (Geneva) and subtropical (Abu Dhabi) climate conditions. The data were calculated based on the temperature- and irradiance-dependent measurements of the different cell architectures and assuming temperature-dependent R_{CTM}. Lines are guides to the eye. The four data points on the right illustrate the trends for four architectures, assuming that $R_{\mathrm{CTM}}^{25^{\circ}\mathrm{C}}$ is between 0.5 $\Omega\,\mathrm{cm}^2$ and 1 $\Omega\,\mathrm{cm}^2$.

References

[1] *American Society of Heating, Refrigerating and Air Conditioning (ASHRAE), Inc., Atlanta, GA, USA www.ashrae.org*, 2001, `https://energyplus.net/weather`.

[2] J. Stein, D. Riley and C. W. Hansen, *PV LIB Toolbox*, 2015, `http://pvpmc.org`.

[3] D. L. King, J. A. Kratochvil and W. E. Boyson, *Online*, 2004, **8**, 1–19.

[4] M. Lave, W. Hayes, A. Pohl and C. W. Hansen, *IEEE Journal of Photovoltaics*, 2015, **5**, 597–606.

[5] P. Loutzenhiser, H. Manz, C. Felsmann, P. Strachan, T. Frank and G. Maxwell, *Solar Energy*, 2007, **81**, 254–267.

[6] C. Gueymard, *Solar Energy*, 1993, **51**, 121–138.

[7] R. Couderc, M. Amara and M. Lemiti, *IEEE Journal of Photovoltaics*, 2016, **6**, 1123 – 1131.

[8] International Standard, *IEC 61724 - Photovoltaic system performance monitoring - Guidelines for measurement, data exchange and analysis*, 1998.